Adsorption (2019) 25:267–278
https://doi.org/10.1007/s10450-018-00006-0

Activated carbons with adsorbed cations as photocatalysts for pollutants degradation in aqueous medium

V. Sydorchuk[1] · O. I. Poddubnaya[1] · M. M. Tsyba[1] · O. Zakutevskyy[1] · O. Khyzhun[2] · S. Khalameida[1] · A. M. Puziy[1]

Received: 18 October 2018 / Revised: 20 December 2018 / Accepted: 24 December 2018 / Published online: 2 January 2019

Abstract
Oxidized activated carbon (AC) based on commercial coconut-shell carbon Aquacarb 607C has been prepared. This AC has micro-mesoporous structure and contains surface carboxyl and phenol/enol groups. Cu- and Co-containing ACs have been synthesized via ion-exchange in acid medium. According to potentiometric titration and XPS data, cation-exchanged forms of AC contain about 0.5% of metal ions. Such cation-containing ACs possess narrowed band gap compared oxidized AC as it is observed for doped oxides. Oxidized and cation-containing ACs have been tested as catalysts in photodegradation of dyes and phenol under UV- and visible irradiation. Initial oxidized AC is photoactive toward rhodamine B and methyl orange under UV illumination but inactive under visible light. For the first time it is shown that cation-exchanged forms of AC have enhanced activity towards rhodamine B, methyl orange and phenol in both UV and visible region. Therefore, the principal possibility of improving the photocatalytic properties of AC by introducing a minimal amount of copper and cobalt cations is shown.

Keywords Activated carbon · Cation-exchanged forms · Photocatalytic degradation · UV and visible irradiation · Decolourisation and mineralization

1 Introduction

Activated carbons (ACs) are high-porous materials with a huge specific surface area. ACs are much more frequently used as a catalyst support than as catalyst on its own (Rodriguez-Reinoso 1998; Trogadas et al. 2014). ACs also are universal and effective adsorbents for removal of organic and inorganic pollutants from gaseous and liquid media, including aqueous solutions (Moreno-Castilla 2004; Radovic et al. 2000). Besides, oxidized ACs possess excellent cation-exchange properties and can bind metal ions (Tarkovskaya 1981; Moreno-Castilla et al. 2004). Therefore, the use of ACs for wastewater purification is based on their adsorption ability (Wong et al. 2018).

Photodegradation of organic pollutants using carbon materials as catalysts can be an alternative technique for water purification (Bagheri et al. 2015; Wang et al. 2014; Lu and Panchapakesan 2006). ACs possessing developed porous structure and adsorption capability also can be prospective in photocatalytic processes, particularly as support of photoactive species or constituent element in compositions with oxides (Trogadas et al. 2014; Bagheri et al. 2015; Wang et al. 2014; Haro et al. 2012; An et al. 2009). However, the photocatalyst must be a semiconductive material with an electronic band structure that can generate electron–hole pairs and others highly reactive radical species after irradiation at a given wavelength (in the visible or UV region). It is known that either a photocatalyst or a molecule is excited by light that has energy greater than the band gap of the semiconductor or the transition energy of an excited state of the molecule, respectively, for a reaction to occur. Carbon materials show different electronic structure: band gap, E_g, is varied in range from the values characteristic for conductors to dielectrics (Mrozowski 1971; Oh et al. 2016). Thus, diamond has E_g = 5.5 eV, i.e. is a semiconductor (Klimm

Electronic supplementary material The online version of this article (https://doi.org/10.1007/s10450-018-00006-0) contains supplementary material, which is available to authorized users.

✉ A. M. Puziy
alexander.puziy@ispe.kiev.ua

[1] Institute for Sorption and Problems of Endoecology, NAS of Ukraine, 13 Naumov St., Kyiv 03164, Ukraine

[2] I.M. Frantsevych Institute for Problems of Materials Science, National Academy of Science of Ukraine, 3 Krzhyzhanovsky St., Kyiv 03680, Ukraine

2014). Graphite is a conductor while graphite oxide as well as graphene oxide are semiconductors with E_g = 1.8–4.7 and E_g = 1.2–4.0 eV, respectively (Jeong et al. 2010; Bustos-Ramírez et al. 2015; Velasco-Soto et al. 2015). Therefore, these solid carbon oxide materials must be photoactive under UV- and visible irradiation, which was confirmed (Bustos-Ramírez et al. 2015; Yeh et al. 2010; Cao et al. 2011).

It is well known that ACs are constructed from aromatic sheets crosslinked in a random manner and contain various oxygen-containing groups in an oxidized state (Rodriguez-Reinoso 1998; Moreno-Castilla 2004; Radovic et al. 2000; Tarkovskaya 1981; Moreno-Castilla et al. 2004). The presence of oxygen-containing groups determine the adsorption, and therefore also photocatalytic properties of ACs to a great extent. Theoretical calculations and experimental measurements showed that ACs can have E_g within 2.9–4.8 eV depending on their origin, chemical composition and mode of preparation (Cao et al. 2011; Bandosz et al. 2012; Strelko et al. 2004; Velo-Gala et al. 2013). In principle, these values allow utilizing ACs as photocatalysts in UV and visible region although there is a limited amount of studies devoted to the photocatalytic properties of ACs where carbon itself acts as catalyst. The application of ACs without semiconductor additives for photocatalytic degradation of organic pollutants in aqueous media were reported earlier (Cao et al. 2011; Bandosz et al. 2012; Velo-Gala et al. 2013; Velasco et al. 2012, 2013). In these works, it has been shown that some ACs were photocatalytically active under UV and visible irradiation. Thus, sulphur-doped carbon showed 2 times higher activity in photodegradation of methylene blue under visible and UV illumination as compared to commercial TiO_2 (Bandosz et al. 2012). Gamma radiation treatment reduces the band gap values of the ACs and increases sodium diatrizoate removal rate under UV light (Velo-Gala et al. 2013). The presence of oxygen-containing groups on the surface is prerequisite for photocatalytic activity of ACs (Bandosz et al. 2012). Nevertheless, the nature of photocatalytic activity of ACs and mechanism of initiating oxidation reactions on carbon surface require further investigations.

In present communication, the activity of oxidized AC and its copper- and cobalt-exchanged forms in photodegradation of dyes and phenol under UV- and visible irradiation were studied. The formulation of the problem is due to several reasons. First, the oxidized AC selectively adsorbs Cu^{2+} and Co^{2+} cations (Radovic et al. 2000; Tarkovskaya 1981; Biniak et al. 1999; Demirbas 2003). Secondly, copper and cobalt oxides are photocatalysts or dopants for semiconductor oxides, first and foremost for titania (Ni et al. 2017; Dhas et al. 2015; Li et al. 2008; Savio et al. 2016). Moreover, copper and cobalt oxides supported on carbons as separate phases are active in different adsorption and oxidation processes, including pollutant degradation (Shu et al. 2017; Park, and; Shin 2004; Zabihi et al. 2015; Shukla et al. 2010). However, ACs doped with copper and cobalt ions as well as with other cations were not yet investigated as photocatalysts. As to authors' knowledge the only study dealt with this topic (Xiaoyan et al. 2011). This work describes photocatalytic degradation of pyrocatechol using Cu_2O/AC catalysts containing 7.15–35.8% of Cu_2O. However, copper (I) oxide forms a separate phase that is a photocatalytically active component while AC, obviously, plays only the role of a support.

2 Experimental

2.1 Materials

Commercial coconut-shell-based AC Aquacarb 607C (Chemviron, Belgium) was oxidized with 20% nitric acid for 5 h. After oxidation, carbon was extensively washed with hot water in a Soxhlet extractor until neutral pH of wash waters and dried at 110 °C. As-obtained oxidized carbon was abbreviated as Ox–H. Copper and cobalt doped carbons were prepared by equilibrating 0.5 g of oxidized carbon Ox–H with 20 mL of 0.01 M solution of corresponding nitrates for 24 h. Initial pH of solution was 2.3 for copper and 2.6 for cobalt nitrates, respectively. After equilibrating carbon was washed with distilled water and dried at 110 °C. Under these conditions, the nitrates are not subjected to hydrolysis. Therefore, adsorption of cations exclusively by ion exchange mechanism was expected. As a result, cation-exchanged types of ACs (Ox–Cu and Ox–Co) were obtained.

2.2 Porous structure

Nitrogen adsorption–desorption isotherms were measured at -196 °C using Autosorb-6 adsorption analyzer (Quantachrome, USA). Pore size distributions (PSD) were calculated by Autosorb-1 software (Quantachrome, USA) using QSDFT method (Gor et al 2012; Landers et al. 2013; Neimark et al. 2009) with a slit/cylindrical pore model. Specific surface area, A_{BET}, was calculated by BET method using nitrogen adsorption data in the relative pressure range chosen by recently proposed procedure (Rouquerol et al. 2007). The total pore volume, V_{tot}, was calculated by converting the amount of nitrogen adsorbed at a maximum relative pressure to the volume of liquid adsorbate. The micropore, V_{mi}, and mesopore, V_{me}, volumes were calculated from the cumulative pore size distribution (PSD) as the volume of pores with sizes less than 2 nm and between 2 and 50 nm, respectively.

2.3 Surface chemistry

Surface chemistry of oxidized carbon Ox–H was investigated by potentiometric titration method (Lützenkirchen

et al. 2012) performed in thermostatic vessel at 25 °C using a DL25 Titrator (Mettler-Toledo, Switzerland). The proton concentration was monitored using an LL pH glass electrode (Metrohm, Switzerland). The method is based on calculation of proton binding from raw potentiometric titration data followed by computation of Proton Affinity Distribution using CONTIN method (Puziy et al. 2001, 2017; Myglovets et al. 2014).

2.4 XPS

All carbon samples were studied by the XPS method in powdered form before and after metal ion uptake. The XPS spectra were measured using the UHV-Analysis-System equipped with a hemispherical PHOIBOS 150 analyzer SPECS Surface Nano Analysis (Berlin, Germany). The XPS spectra were measured in an ion-pumped chamber of the System at a base pressure less than 8×10^{-10} mbar. The spectra were excited by a Mg Kα source of X-ray radiation ($E = 1253.6$ eV) and were acquired at constant pass energy of 30 eV. The binding energy scale was calibrated by assigning 284.6 eV to the C 1s line (Khyzhun et al. 1996, 2013).

2.5 FTIR

The FTIR reflectance spectra in the range 4000–400 cm^{-1} for ACs were registered using the "Spectrum-One" spectrometer (Perkin-Elmer). The ratio of sample and KBr powders was 1:250.

2.6 Diffuse reflectance spectra

Diffuse reflectance spectra (DRS) of the powdered ACs were registered using spectrometer Shimadzu UV-2450. Base-line spectra were obtained from a sample of pressed barium sulfate. ACs samples for spectra registration were prepared by diluting the ACs with barium sulfate at a ratio of 1:10 in accordance with the methodology described in detail in the work (Velo-Gala et al. 2013). This methodology is based on Kubelka–Munk equation. To authors' knowledge this is the only study in which the absorption edge for ACs was experimentally measured and band gap was calculated.

2.7 Photocatalytic tests

Photocatalytic degradation under visible irradiation was performed in a glass reactor. LED Cool daylight lamp (Philips, 100 W) with emission spectra exclusively in the visible range with broad maximum in the region 500–700 nm and local maximum around 440 nm was used as illumination source (Fig. 1S). UV-photocatalytic degradation was realized in quartz reactor using low pressure Hg lamp with emission maximum at 254 nm, local maximum at 185 nm and power 30 W. The solution before and after substrates degradation were analyzed spectrophotometrically (Shimadzu UV-2450) at $\lambda_{max} = 553$, 461 and 265 nm for rhodamine B (RhB), methyl orange (MO), and phenol (Ph), respectively, after centrifugation of reaction mixture (10 min at 8000 rpm). The initial concentrations of RhB, MO and Ph were $1–3 \times 10^{-5}$ mol L^{-1}, $1–2 \times 10^{-5}$ mol L^{-1}, and 10 mg L^{-1} (1.06×10^{-4} mol L^{-1}), respectively. First, the dark adsorption of all substrates was studied to determine the time needed to establish the adsorption equilibrium. It should be noted that photolytic degradation of all substrates even under the influence of UV radiation does not exceed 5%. The calculation of photodegradation rate K_d (K_d^{UV} und K_d^{Vis} for reactions under UV and visible illumination, respectively) was based on the temporal changes of optical density D (substrate concentration) after reaching the adsorption equilibrium in dark. The obtained results are satisfactorily described by the first-order kinetic equation ($R^2 = 0.88–0.98$). The control of pH value during photocatalytic reaction was performed using apparatus pH-150M. The total organic carbon (TOC) for selected solutions was measured using a Shimadzu TOC analyzer (model 5050A).

3 Results and discussion

3.1 Porous structure

Nitrogen adsorption–desorption isotherms for oxidized carbon Ox–H (Fig. 1a) can be attributed to a combination of type I and type IVa of IUPAC classification (Thommes et al. 2015). A steep raise of nitrogen uptake at very low p/p_0 is due to adsorption in narrow micropores with enhanced potential while gradual increase in nitrogen adsorption at medium to high relative pressures corresponds to monolayer-multilayer adsorption in mesopores followed by capillary condensation accompanied by small hysteresis of type H4. The isotherm is typical to micro-mesoporous carbons. Pore size distribution of oxidized carbon Ox–H (Fig. 1b) shows two sharp peaks corresponding to micropores (1.1 nm) and mesopores (2.2 nm). Oxidized carbon Ox–H shows high specific surface area of 1070 $m^2 g^{-1}$ with a total pore volume of 0.45 $cm^3 g^{-1}$ distributed in micropores (82%) and mesopores (18%). Since cation-exchanged forms contain few amount of metals (as will be shown below), the isotherms and PSD curves obtained for Ox–Cu and Ox–Co samples practically do not differ from those for the Ox–H and therefore are not shown here.

3.2 Surface chemistry

Proton-binding isotherm for oxidized carbon Ox–H (Fig. 2a) decreases with increasing pH due to gradual

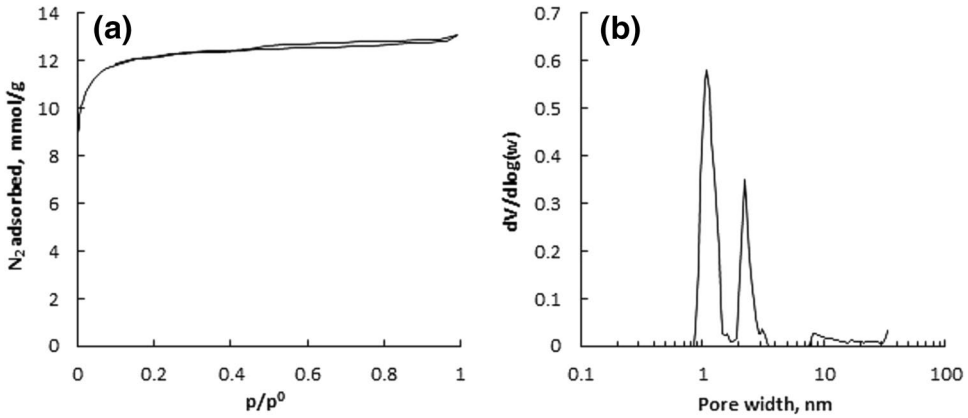

Fig. 1 Nitrogen adsorption isotherm (**a**) and pore size distribution (**b**) for oxidized carbon Ox–H

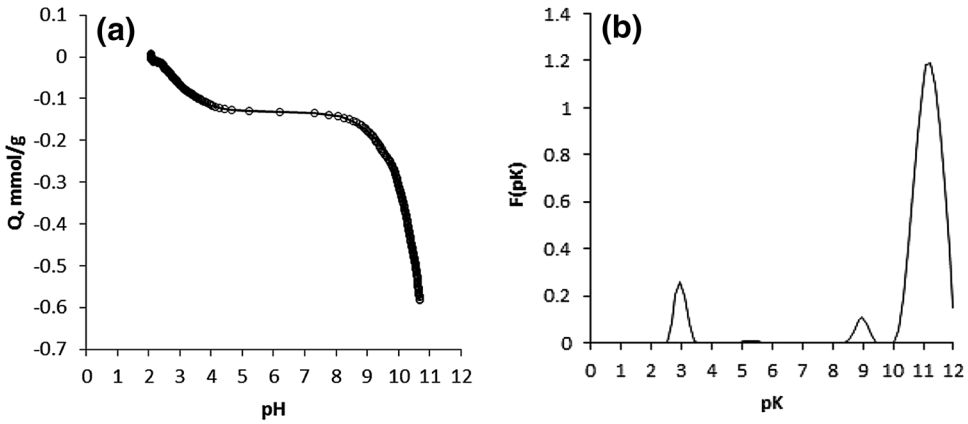

Fig. 2 Proton-binding isotherm (**a**) and proton affinity distribution (**b**) for oxidized carbon Ox–H

dissociation of surface groups. Point of zero charge, where proton binding is zero, lies at 2.09 showing negatively charged surface of carbon at pHs of adsorption of metal ions. The shape of proton-binding isotherm for oxidized carbon Ox–H is characteristic to multifunctional cation exchangers containing surface groups of different acidity.

Proton affinity distribution of acid groups calculated by CONTIN method shows four peaks for oxidized carbon Ox–H (Fig. 2b). The peaks may be classed as strong carboxylic (0.13 mmol g^{-1}, pK 3.0), weak carboxylic (0.01 mmol g^{-1}, pK 5.3) and two types of phenolic and/or enol groups (0.06 mmol g^{-1}, pK 9.0; 1.32 mmol g^{-1}, pK 11.2). Total amount of surface groups, 1.52 mmol g^{-1}, corresponds to an oxygen content of 2.7%. Based on the assumption that metal ions are bound to strong carboxyl groups at experimental pH (Myglovets et al. 2014; Khyzhun et al. 1996) and taking into account the amount of strong carboxylic groups, the content of copper and cobalt in the cation-exchanged forms is estimated as 0.42% and 0.38%, respectively.

XPS survey scans showed the presence of carbon, oxygen and modifying metals (Fig. 3; Table 1). The oxygen content is about 9% for all carbons due to oxidation with nitric acid. The amount of heavy metals was about 0.5% which is

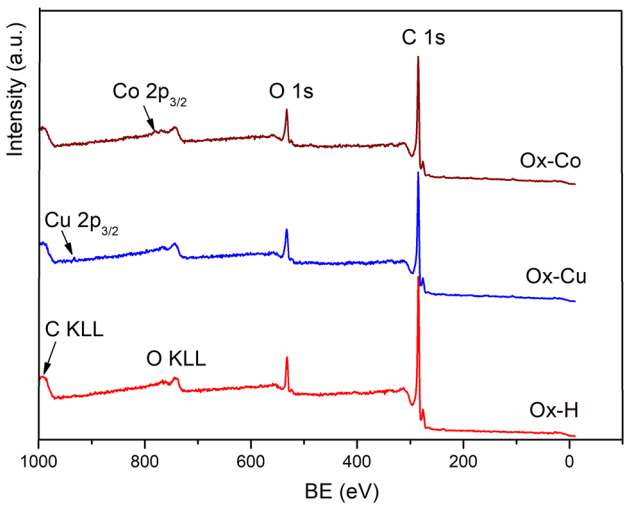

Fig. 3 Survey XPS spectra for samples Ox–H, Ox–Cu, Ox–Co

satisfactorily in line with calculations from content of strong carboxylic groups.

High-resolution XPS spectra of C 1 s excitation showed complicated envelope that indicated several carbon species at the carbon surface (Fig. 4a). The spectra were deconvoluted

Table 1 Mass concentration of the elements and relative concentration of the components of C1s and O1s envelopes

Peak component	Ox–H	Ox–Cu	Ox–Co
Survey			
C	91.0	90.6	90.5
O	9.0	8.9	9.0
Cu		0.5	
Co			0.5
C1s			
sp^2 (284.3–284.4 eV)	41%	47%	50%
C–O (285.4–285.6 eV)	44%	29%	33%
C=O (287.1–288.2 eV)	10%	21%	14%
$\pi \rightarrow \pi^*$ (290.6–291.4 eV)	4%	4%	3%
O1s			
C=O (531.0–531.1 eV)	10%	18%	11%
C–O (532.5–532.9 eV)	70%	41%	73%
H_2O (534.0–535.4 eV)	20%	40%	15%

into four components adopted in the analysis of carbon materials (Biniak et al. 1999; Puziy and Poddubnaya 1998; Puziy et al. 2006, 2008; Estrade-Szwarckopf 2004). The components represent sp^2-hybridized carbon, carbon singly bonded to oxygen (C–O), carbon doubly bonded (C=O) to oxygen and $\pi \rightarrow \pi^*$ transition (Table 1). Adsorption of heavy metals caused changes in chemical environment of C atoms which is reflected in decreasing C–O component and increasing C=O component (Fig. 4b, c). The stronger impact on redistribution of C1s components is observed for copper.

O1s peak for oxidized AC (Fig. 5a) was deconvoluted to three components assigned to oxygen double bonded to carbon (C=O), to singly bonded oxygen (–O–) in C–O and to chemisorbed oxygen and water (Biniak et al. 1999; Puziy et al. 2008; Moulder et al. 1992). The presence of copper altered chemical environment of oxygen atoms, which resulted in increasing contribution of doubly bonded oxygen and decreasing relative amount of singly bonded oxygen (Fig. 5b) while impact of cobalt is much smaller (Fig. 5c). These findings are in line with observations from the C1s components (Fig. 4a, b).

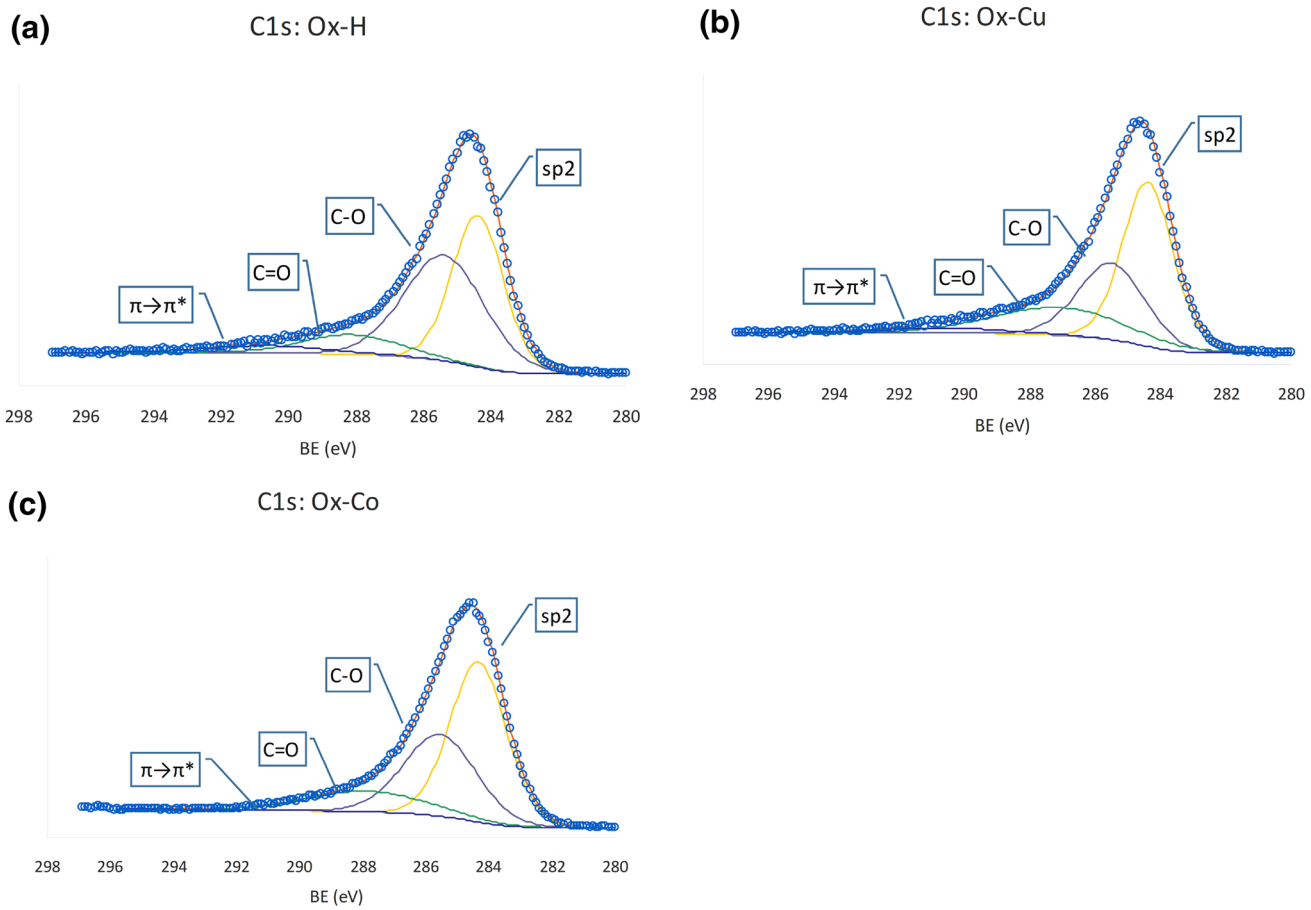

Fig. 4 C1s XPS spectra for Ox–H (**a**), Ox–Cu (**b**), Ox–Co (**c**) samples

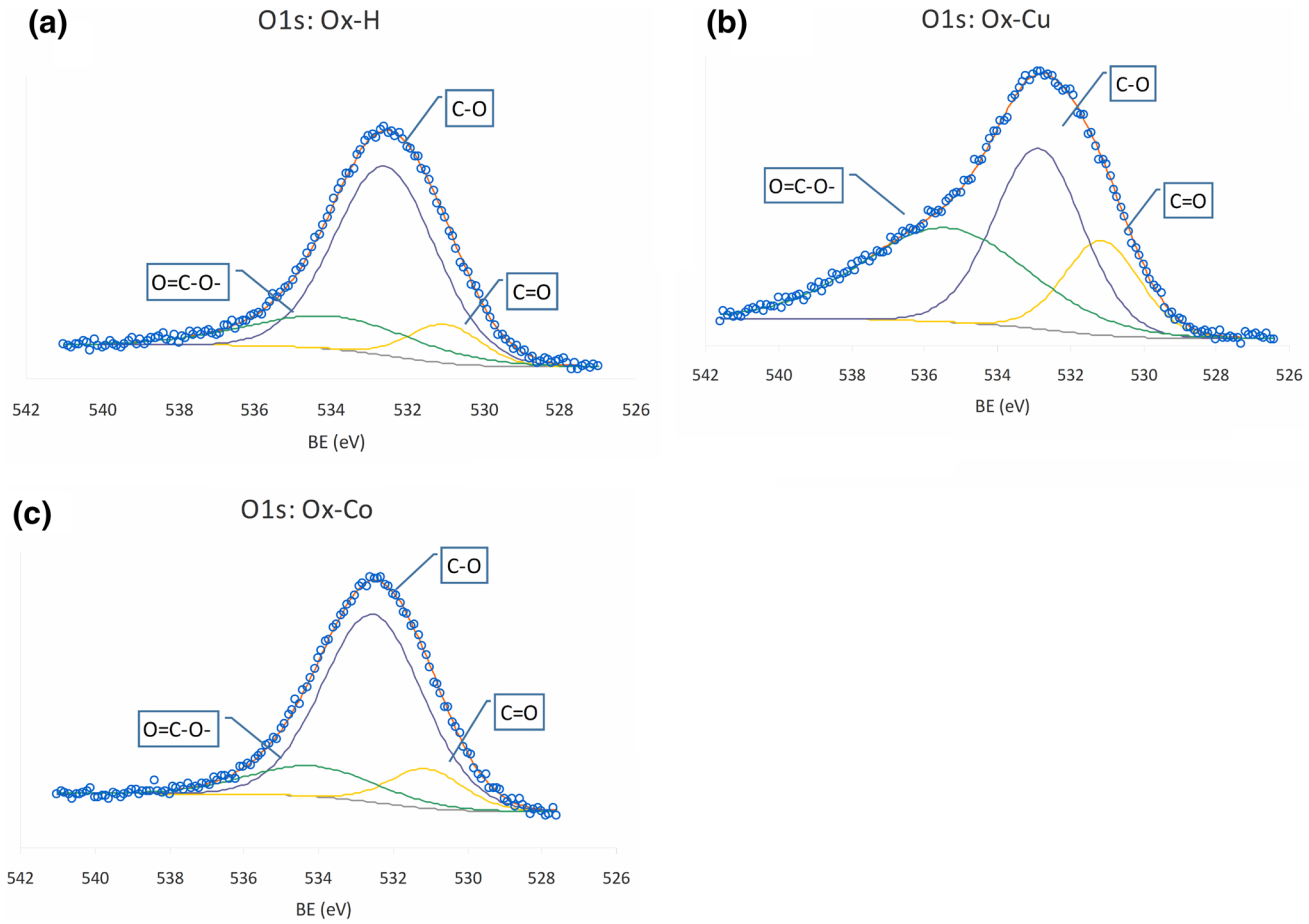

Fig. 5 O1s XPS spectra for Ox–H (**a**), Ox–Cu (**b**), Ox–Co (**c**) samples

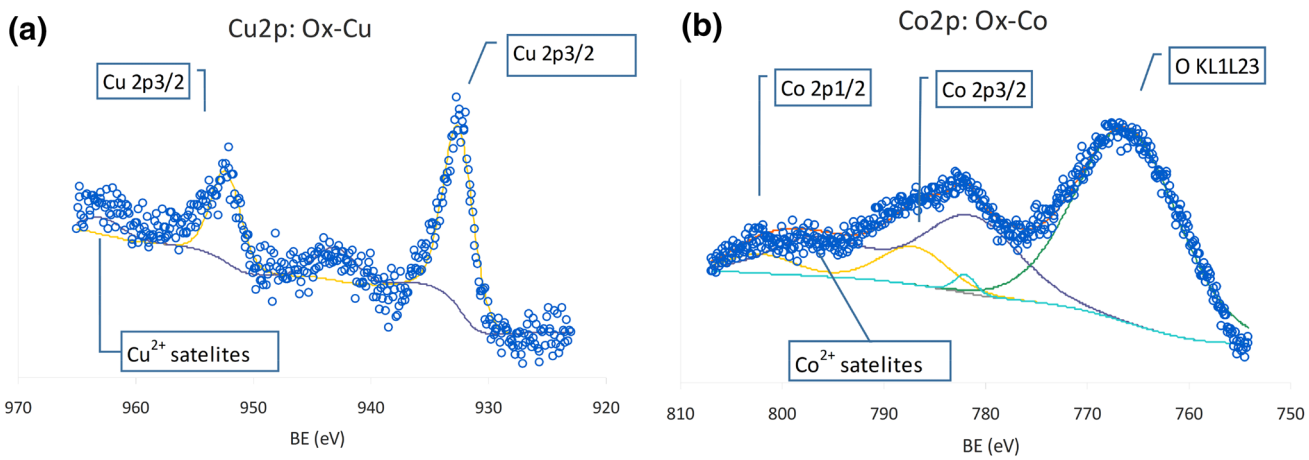

Fig. 6 Cu2p XPS spectrum for Ox–Cu sample (**a**) and Co2p spectrum for Ox–Co sample (**b**)

High resolution XPS spectra from metal-containing carbons showed Cu 2p (bond energy BE 932.6 eV) and Co 2p (781.5 eV) peaks (Fig. 6a, b), which correspond to Cu(II) and Co(II) species, respectively (Li et al. 2008; Shu et al. 2017; Zabihi et al. 2015; Shukla et al. 2010; Khyzhun et al. 2005; Rajagopal et al. 2010). The presence of relatively strong satellite peak for Cu (943.0 eV) confirms valence state of copper as 2+ (Shu et al. 2017; Park and Shin, 2014). From the above it appears that copper and cobalt occupy cation-exchange positions.

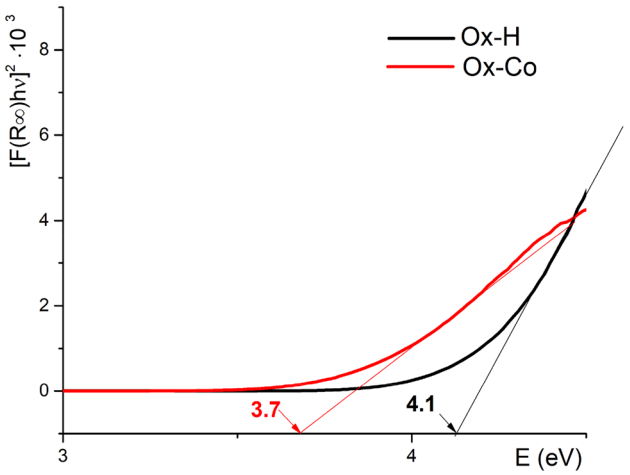

Fig. 7 The Tauc plots for Ox–H and Ox–Co samples

3.3 Diffuse reflectance spectra

The Tauc plots for oxidized AC and its Co-exchanged form (Ox–H and Ox–Co, respectively) are presented in Fig. 7. It can be seen that bang gap E_g for Ox–H sample is 4.1 eV. Such a high value can be associated with a relatively low content of oxygenated groups, namely about 2.7% w/w (see above) although total content of oxygen is about 9% due to adsorbed forms of oxygen (XPS data, Table 1). Indeed, from the relationship between E_g value and total oxygen content, which was obtained by the authors of work (Velo-Gala et al. 2013) for ACs, it follows that the value of the band gap for Ox–H sample should be higher than 4 eV. Introduction of Cu and Co into the carbon structure causes the narrowing of band gap to 3.9 and 3.7 eV, respectively. This is a known doping effect, which is well studied for oxides (Ni et al. 2017; Dhas et al. 2015). The obtained values of band gap show the semiconductor nature of the studied ACs. It seems that the order of this magnitude, as well as the established tendency of its changes after introduction of metals, are the most important results that explain the photocatalytic properties of ACs.

3.4 Dose of carbon photocatalyst and substrate concentration

Since ACs have high specific surface area and, consequently, high adsorption capacity, the optimal content in reaction mixture is much less, than that for oxide photocatalysts. Recent studies (Bandosz et al. 2012; Velo-Gala et al. 2013; Velasco et al. 2013) used 0.05–0.2 g L^{-1} of AC, while the content of 1–2 g L^{-1} is optimal for processes using TiO_2 as photocatalyst (Kapinus et al. 2009; Gupta et al. 2007). It is well known that adsorption at the surface of catalysts (including photocatalyst) is the first stage of the catalytic processes. We found that adsorption of dyes by AC catalyst reaches 90–95% when the content of AC is 0.15–0.2 g L^{-1}. Therefore, we used for all experiments the content of AC equal to 0.1 g L^{-1} as optimal. In this case, adsorption of dyes and phenol is 40–75% and 25–30% (depending on substrate concentration), respectively. The difference in adsorption is obviously because molecules of RhB and MO contain basic groups and could be specifically adsorbed onto acid surface of AC. On the other hand, phenol has only acidic group and hence phenol is less adsorbed on an acidic surface of AC. Indeed, the pH values are 6.9, 6.8 and 4.7 for initial solutions of RhB, MO and Ph, respectively. From proton binding curve (Fig. 2a) it follows that carbon Ox–H shows about 0.13 mmol g^{-1} of dissociated acid groups at pHs of substrate adsorption. Adsorption equilibrium was established for 2 h for all substrates (Fig. 8). These results are consistent with the data from other studies devoted to photocatalytic degradation of dyes using ACs (Bandosz et al. 2012; Velo-Gala et al. 2013; Velasco et al. 2012).

The influence of substrate concentration on photocatalytic activity of ACs samples was also studied. Thus, the dependence between RhB concentration and catalytic activity of Ox–Cu was established: K_d^{UV} value monotonically diminishes from 9.4 to 1.4×10^{-4} s^{-1} when RhB concentration increases within $1–2 \times 10^{-5}$ mol L^{-1}. It should be noted that this is a well-known and obvious pattern for photocatalytic processes. All carbon catalysts become inactive at the RhB concentration 3.0×10^{-5} mol L^{-1}. It is obviously that this is due to the blocking of active surface centers by the adsorbed dye. As a result, the most suitable concentrations for photocatalytic testing were found as following: 1.8×10^{-5} mol L^{-1}, 2.0×10^{-5} mol L^{-1}, 1.06×10^{-4} mol L^{-1} for RhB, MO and phenol, respectively. As mentioned above photolysis of these substrates even under UV irradiation is not more than 5%.

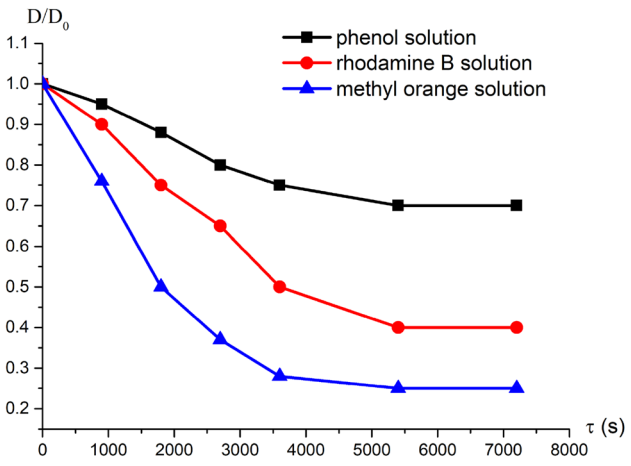

Fig. 8 Kinetic curves of substrates adsorption in dark by carbon Ox–H

Table 2 The values of rate constant degradation at optimal concentration of substrates

N	Photocatalyst	Substrate	$K_d^{UV} \times 10^4$ (s^{-1})	$K_d^{Vis} \times 10^4$ (s^{-1})
1	AC Ox–H	RhB	1.8	Inactive
2	AC Ox–Cu	RhB	2.7	1.2
3	AC Ox–Co	RhB	2.9	0.5
4	AC Ox–H	MO	0.1	Inactive
5	AC Ox–Cu	MO	0.3	0.6
6	AC Ox–Co	MO	0.6	0.5
7	AC Ox–H	Phenol	Inactive	Inactive
8	AC Ox–Cu	Phenol	0.15	0.1
9	AC Ox–Co	Phenol	0.24	0.1

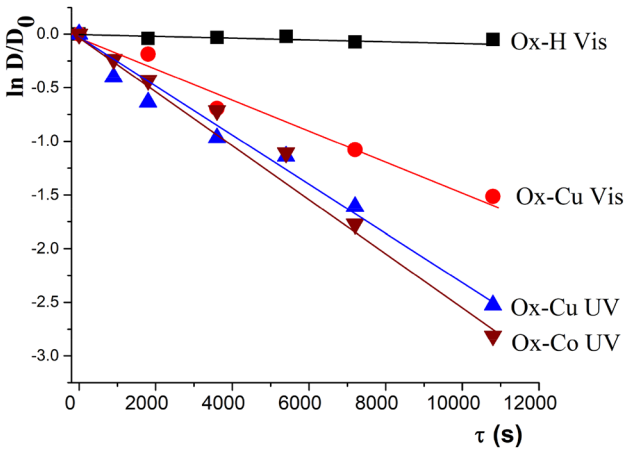

Fig. 9 Kinetic curves of RhB degradation for Ox–H Vis, Ox–Cu Vis, Ox–Cu UV, Ox–Co UV

3.5 Photocatalytic degradation of RhB

First, RhB was tested as substrate because the spectrum of its absorption is overlapped in a wide region with the emission spectrum of lamp—illumination source (Fig. 1S): the maxima are located at 553 and 565 nm, respectively. Therefore, the absorption of light and the direct excitation of dye molecules without the participation of a photocatalyst are very likely, at least the most probable of all the substrates used.

It is necessary to note that initial oxidized carbon Ox–H predictably has no photocatalytic activity under visible illumination but exhibits noticeable activity under UV irradiation (Table 2; Fig. 9). The photocatalytic properties of oxidized carbon are improved after introduction of Cu^{2+} and Co^{2+} cations into its structure (Fig. 9). K_d^{UV} value for these doped samples is practically the same (within measurement error) and increases by one and a half times compared with Ox–H sample (Table 2). The electron spectrum of RhB does not changed under UV irradiation, only intensity of band at 553 drastic decreases (Fig. 2S). Under UV irradiation, Ox–Cu sample showed somewhat less photocatalytic activity as compared with Ox–Co since the former carbon has larger value of band gap E_g than the latter. On the contrary, Ox–Cu is more active under visible light (Table 2). It should be also noted that Ox–Cu and Ox–Co samples can be re-used three cycles without loss of activity in degradation of RhB under UV illumination. The activity in the third cycle is at least 90–95% of that for the fresh samples.

MO has maximum of absorption at 461 nm. So, its absorption spectrum to a minimum degree overlaps with the emission spectrum of the used lamp. At the same time, maximum of absorption for phenol is located in the UV region, namely at 265 nm. The character of the changes in the spectrum during the degradation of MO and Ph is shown in Fig. 10a, b. Monotonic decrease of band at 461 nm is observed with an increase in the duration of UV irradiation of MO solution. Besides, a slight blue shift of the absorption maximum (up to 445 – 442 nm) for MO is seen after 6–8 h illumination. The kinetic curve of this process is presented in Fig. 11. Similar spectra and kinetic curves were obtained for the photocatalytic degradation of phenol (Figs. 10b, 11, respectively): as can be seen intensity of band at 265 nm decreases 4 times for 7 h. Based on these results, kinetic curve of Ph degradation, which well described by first-order equation, was plotted.

The rate constant of degradation calculated for these processes as well as for visible photocatalytic degradation are also presented in Table 2.

3.6 Discussion

Initial oxidized carbon (Ox–H) showed activity toward the RhB and MO only under the action of UV light. From the data of spectrophotometric measurements, it can also be seen that photocatalytic processes using Cu- and Co-containing carbons result in degradation of substrates under both UV- and visible illumination. The optical density of dye solutions after illumination (D) reduces 4–12 times for 7 h compared with that for solutions after adsorption (D_0). Therefore, the degree of dye discoloration reaches 90–95% for catalysts with highest activity. At the same time, decreasing in TOC value is a measure of pollutants total mineralization (Rauf and Ashraf 2009). In our case, the degree of mineralization calculated on the base of TOC values is within 16–73%. Moreover, the comparison of FTIR spectra for Ox–Cu catalyst (Fig. 12) indirectly indicate possibility of degradation of adsorbed RhB. Thus, spectrum after RhB adsorption contains broad poorly resolved absorption bands in the region 950–1350 cm^{-1} where there are characteristic absorption bands for RhB. At the same time, these absorption bands are absent in the spectrum of the

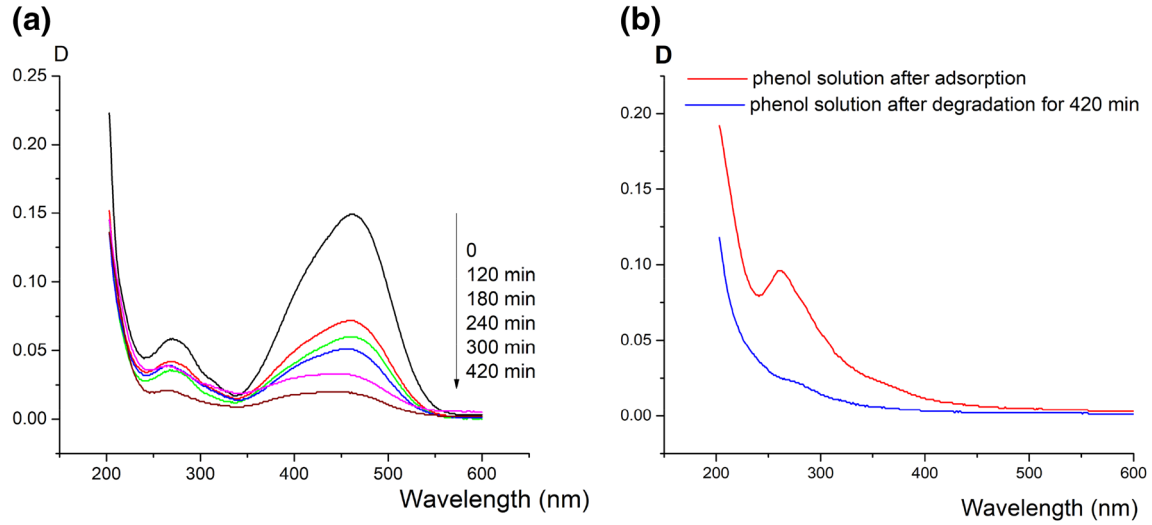

Fig. 10 The absorption spectra of MO solution after degradation under UV irradiation in the presence of Ox–Co (**a**) and phenol solution after adsorption and degradation for 420 min under UV irradiation (**b**)

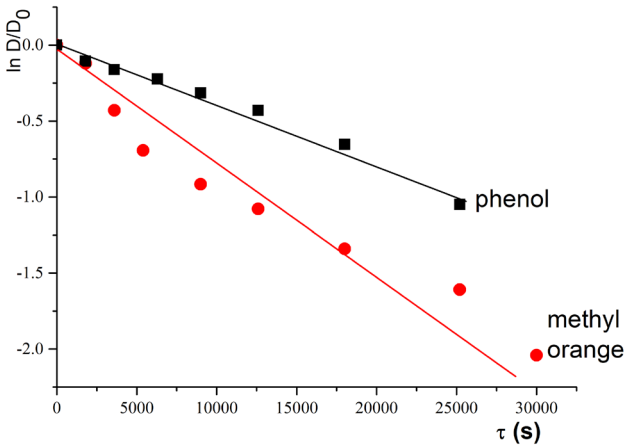

Fig. 11 The kinetic curves of photocatalytic degradation of phenol and methyl orange under UV illumination using Ox–Co as catalyst

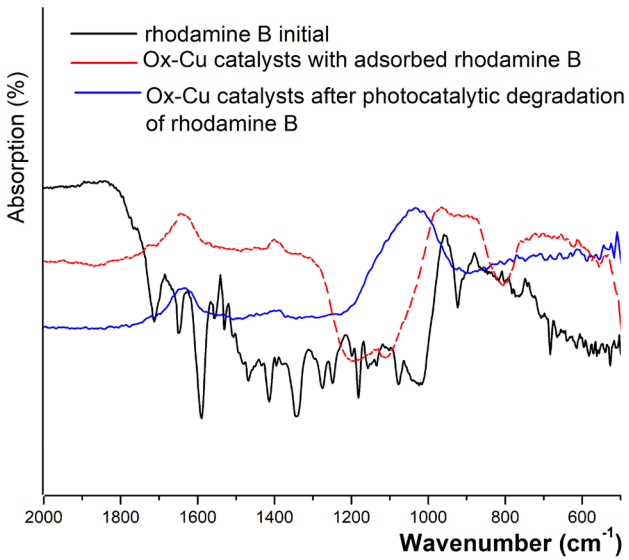

Fig. 12 FTIR spectra for initial RhB, Ox–Cu catalyst with adsorbed RhB and the same after phocatalysis

same sample after photocatalysis. This fact provides support for disappearance of RhB at the carbon surface after photodegradation.

There are several mechanisms for initiation of photocatalytic processes. The contribution of each of them to the resulting overall effect depends on the nature of the substrate and the photocatalyst, as well as on the type of used irradiation. Thus, when a catalyst is exposed to radiation with energy equal or higher than band gap, electrons are promoted from the valence band to the conduction band. As a result, an electron–hole pairs are produced and photoactive species (likely $OH^{\bullet}$ radicals) generated which initiate the processes of substrate oxidation. This well-known mechanism was described in detail in the literature (Xiaoyan et al. 2011; Rauf and Ashraf 2009) and therefore is not discussed here. UV degradation of RhB, MO and Ph on all carbons obviously occurs according to similar mechanism since energy of photons is within 3.6–6.7 eV while band gap values for oxidized and cation-exchanged carbons are 4.2 and 3.9 eV, respectively. Due to the narrowing of the band gap for metal-containing carbons, the rate of degradation of all studied substrates is higher as compared with Ox–H (Table 2). Besides, the photocatalytic activity of the cation-exchanged carbons can be favored not only by the decrease in E_g values but also by the amount of carbon atoms with sp^2 hybridization state as suggested in Velo-Gala et al. (2013). As can be seen from Table 1, the content of C1s with sp^2

hybridization increases from 41% for Ox–H to 47% and 50% for Ox–Cu and Ox–Co, respectively. Photocatalytic activity increases under the action of UV light in the same order confirming experimentally the assumption made in Velo-Gala et al. (2013). Taking into account the fact of low metal content, it can also be assumed that small additions of metals can act as nanodots similar to the results of works (Demirbas 2003; Ni et al. 2017).

On the other hand, visible irradiation with energy of photons less than 3.3 eV does not promote the formation of electron–hole pairs. Nevertheless, as indicated above, the cation-containing carbons show photocatalytic activity in degradation of all studied substrates. Obviously, other mechanisms are involved for initiation of oxidation processes under visible light. The maximal rate of degradation is observed for rhodamine B. This may be due to the fact that RhB molecules absorb visible light photons and their excitation is possible, i.e. photosensitization is realized (Xiaoyan et al. 2011; Rauf and Ashraf 2009; Wu et al. 1998): in this case the excitation of dye molecules occurs and excited adsorbed molecules of dye inject electron to conduction band of the catalyst. As a consequence, active species at the catalyst surface are generated. This mechanism of photocatalytic process initiation was also described (Rauf and Ashraf 2009; Wu et al. 1998; Sangami and Dharmaraj 2012).

It is also well-known that photocatalytic degradation of RhB can occur by two pathways (Wu et al. 1998; Sangami and Dharmaraj 2012): (i) as de-ethylation process in a stepwise manner with the formation of the three intermediates from RhB to completely de-ethylated Rh110 or (ii) as a direct cleavage of the chromophore rings. The gradual blue shift in λ_{max} on spectrum of RhB is observed in the first case and the reduction in the absorbance without shift takes place in the second case. As can be seen from Fig. 2S, the RhB degradation in the presence carbon photocatalyst occurs in accordance with the second route: only decrease in intensity of band at 553 nm is observed. Simultaneously, reduction in intensity of band in UV region, namely around 260 nm, takes place (Fig. 2S). The latter indicates the destruction of benzene rings in the dye molecules (Merka et al. 2011). The same results were obtained using all photocatalysts under UV and visible illumination. The similar findings were described for degradation of rhodamine B and safranin T using vanadium and molybdenum oxides as photocatalysts (Sydorchuk et al. 2013).

The lowest values of photodegradation rate constant K_d are obtained for MO and phenol (Table 2). This may be due to a decrease in the role of the photosensitization process because the absorption spectra of these substances are minimally overlapped with emission spectrum of the lamp for visible region (Fig. 1S). This is especially true for phenol. It is possible that absorbed energy causes oxidation of substrates as observed in the wet oxidation of phenol on ACs, including copper-containing catalyst (Santos et al. 2005; Moreno-Piraján and Giraldo 2013). Such an alternative mechanism of photocatalytic oxidation initiation can be connected with formation of several radical species at the surface of carbon in contact with aqueous solution containing dissolved oxygen (Velo-Gala et al. 2013; Hayyan et al. 2016; Boehm 2012):

$$O_2 + e_{carbon}^- \rightarrow O_2^{\cdot -}$$
$$O_2^{\cdot -} + H_2O \rightarrow HO_2^{\cdot} + HO^-$$
$$2HO_2^{\cdot} \rightarrow O_2 + H_2O_2 \rightarrow O_2 + 2HO^{\cdot}$$

Indeed, XPS showed that more than 60% of total oxygen is in the adsorbed state. It is well known that superoxide ion takes an important part in oxidation reactions *via* interaction with adsorbed molecules of substrates (Strelko et al. 2004, 2000; Xiaoyan et al. 2011; Matzer and Boehm 1998; Hayyan et al. 2016), including in photocatalytic processes (Tang et al. 2018; Xu et al. 2018). $HO^{\cdot}$ radicals, as active species of all photocatalytic processes, can also be produced by the disproportionation of $O_2^{\cdot}-$ ions.

4 Conclusions

Initial oxidized AC has micro-mesoporous structure with predominance of micropores and contains four types of surface acidic groups. Cu- and Co- containing ACs were prepared via cation exchange with protons of surface carboxylic groups. Metal-doped carbons are characterized by narrower band gap compared with oxidized carbon and increased content of carbon with sp^2 hybridization.

Initial oxidized AC is photocatalytically active towards dyes (RhB and MO) under UV illumination but inactive under visible light. Cation-exchanged forms of AC like doped semiconductor oxides have narrowed band gap and improved photocalytic activity (compared with initial AC) in the degradation of dyes and phenol under UV and visible irradiation. The substrates can be graded in the degree of degradation under UV irradiation: RhB > MO > Ph.

It is important that the degradation is accompanied by partial mineralization of substrates. For 7 h irradiation, the degree of discoloration of dye solutions reaches 90–95% and degree of mineralization for dyes and phenol in solutions (according to TOC measurements) is 16–73%. The practical significance of the results obtained is that spent carbons with adsorbed cations, instead of regeneration, can be re-used in photocatalytic degradation of pollutants in aqueous media. As a result, the formation of secondary contaminated water during regeneration is prevented. Besides, a low content of carbon photocatalysts in the reaction mixture (practically

an order of magnitude smaller than that of oxide photocatalysts) is their additional advantage. Therefore, two problems can be solved simultaneously, namely re-using spent carbon cation exchanger and the purification of water from organic pollutants.

Acknowledgements Funding was provided by National Academy of Sciences of Ukraine (Grant No. 35NT).

References

An, G., Ma, W., Sun, Z., Liu, Z., Han, B., Miao, S., Miao, Z., Ding, K.: Preparation of titania/carbon nanotube composites using supercritical ethanol and their photocatalytic activity. Carbon **45**, 1795–1801 (2009)

Bagheri, S., Julkapli, N., Hamid, A.S.: Functionalized activated carbon derived from biomass for photocatalysis applications perspective. Int. J. Photoenergy. 2015. https://doi.org/10.1155/2015/218743 (2015)

Bandosz, T., Matos, J., Seredych, M., Islam, M., Alfano, R.: Photoactivity of S-doped nanoporous activated carbons: a new perspective for harvesting solar energy on carbon-based semiconductors. Appl. Catal. A **445–446**, 159–165 (2012)

Biniak, S., Pakuła, M., Szymański, G., Świątkowski, A.: Effect of activated carbon surface oxygen- and/or nitrogen-containing groups on adsorption of copper(II) ions from aqueous solution. Langmuir **15**, 6117–6122 (1999)

Boehm, H.: Free radicals and graphite. Carbon **50**, 3154–3157 (2012)

Bustos-Ramírez, K., Barrera-Díaz, E., De Icaza-Herrera, C., Martínez-Hernández, M., Natividad-Rangel, A., Velasco-Santo, R.C.: 4-chlorophenol removal from water using graphite and graphene oxides as photocatalysts. J. Environ. Health Sci. Eng. **13**, 13–33 (2015)

Cao, L., Sahu, S., Anilkumar, P., Bunker, C., Xu, J., Shiral Fernando, K., Wang, P., Guliants, E., Tackett, I.I., Sun, K., Ya, P.: Carbon nanoparticles as visible-light photocatalysts for efficient CO_2 conversion and beyond. J. Am. Chem. Soc. **133**, 4754–4757 (2011)

Demirbas, E.: Adsorption of cobalt(II) ions from aqueous solution onto activated carbon prepared from hazelnut shells. Adsorp. Sci. Technol. **21**, 951–963 (2003)

Dhas, C., Venkatesh, R., Jothivenkatachalam, K., Nithya, A., Suji Benjamin, B., Ezhil Raj, M., Jeyadheepan, A., Sanjeeviraja, K.C.: Visible light driven photocatalytic degradation of Rhodamine B and Direct Red using cobalt oxide nanoparticles. Ceram. Int. **41**, 9301–9313 (2015)

Estrade-Szwarckopf, H.: XPS photoemission in carbonaceous materials: a "defect" peak beside the graphitic asymmetric peak. Carbon **42**, 1713–1721 (2004)

Gor, G., Thommes, M., Cychosz, A., Neimark, A.: Quenched solid density functional theory method for characterization of mesoporous carbons by nitrogen adsorption. Carbon **50**, 1583–1590 (2012)

Gupta, V., Jain, R., Mittal, A., Mathur, M., Sikarwar, S.: Photochemical degradation of the hazardous dye Safranin-T using TiO_2 catalyst. J.Colloid Interface Sci. **309**, 464–469 (2007)

Haro, M., Velasco, L., Ania, C.: Carbon-mediated photoinduced reactions as a key factor in the photocatalytic performance of C/TiO_2. Catal. Sci. Technol. **2**, 2264–2272 (2012)

Hayyan, M., Hashim, M., Alnashef, I.: Superoxide ion: generation and chemical implications. Chem. Rev. **116**, 3029–3085 (2016)

Jeong, H., Yang, C., Kim, B., Kim, K.-J.: Valence band of graphite oxide. Europhys. Lett. **92**, 37005-p1–37005-p4 (2010)

Kapinus, E., Viktorova, T., Khalyavka, T.: Dependence of the rate of photocatalytic decomposition of safranine on the catalyst concentration. Theor. Exp. Chem. **45**, 114–117 (2009)

Khyzhun, O., Zhurakovsky, E., Sinelnichenko, A., Kolyagin, V.: Electronic structure of tantalum subcarbides studied by XPS, XES, and XAS methods. J. Electron Spectrosc. Relat. Phenom. **82**, 179–192 (1996)

Khyzhun, O., Strunskus, T., Cramm, S., Solonin, Y.: Electronic structure of $CuWO_4$: XPS, XES and NEXAFS studies. J. Alloys Compd. **389**, 14–20 (2005)

Khyzhun, O., Bekenev, V., Atuchin, V., Galashov, E., Shlegel, V.: Electronic properties of $ZnWO_4$ based on ab initio FP-LAPW band-structure calculations and X-ray spectroscopy data. Mater. Chem. Phys. **140**, 588–595 (2013)

Klimm, D.: Electronic materials with a wide band gap: recent developments. Int. Union Crystallogr. J. **1**, 281–290 (2014)

Landers, J., Gor, G., Neimark, A.: Density functional theory methods for characterization of porous materials. Colloids Surf. A **437**, 3–32 (2013)

Li, G., Dimitrijevic, N., Chen, L., Rajh, T., Gray, K.: Role of surface/interfacial Cu^{2+} sites in the photocatalytic activity of coupled $CuO\text{-}TiO_2$ nanocomposites. J. Phys. Chem. C **112**, 19040–19044 (2008)

Lu, S., Panchapakesan, B.: Photoconductivity in single wall carbon nanotube sheets. Nanotechnology **17**, 1843–1850 (2006)

Lützenkirchen, J., Preočanin, T., Kovačević, D., Tomišić, V., Lövgren, L., Kallay, N.: Potentiometric titrations as a tool for surface charge determination. Croat. Chem. Acta **85**, 391–417 (2012)

Matzer, S., Boehm, H.: Influence of nitrogen doping on the adsorption and reduction of nitric oxide by activated carbons. Carbon **36**, 1697–1709 (1998)

Merka, O., Varovyi, Y., Bahnemann, D., Wark, M.: pH-control of the photocatalytic degradation mechanism of Rhodamine B over $Pb_3Nb_4O_{13}$. J. Phys. Chem. C **115**, 8014–8023 (2011)

Moreno-Castilla, C.: Adsorption of organic molecules from aqueous solutions on carbon materials. Carbon **42**, 83–94 (2004)

Moreno-Castilla, C., Alvarez-Merino, M., López-Ramón, M., Rivera-Utrilla, J.: Cadmium ion adsorption on different carbon adsorbents from aqueous solutions. Effect of surface chemistry, pore texture, ionic strength, and dissolved natural organic matter. Langmuir **20**, 8142–8148 (2004)

Moreno-Piraján, J., Giraldo, L.: Comparison of the oxidation of phenol with iron and copper supported on activated carbon from coconut shells. Arab. J. Sci. Eng. **38**, 49–57 (2013)

Moulder, J., Stickle, W., Sobol, P., Bomben, K.: Handbook of X-ray Photoelectron Spectroscopy, 2nd edn. Perkin-Elmer, Eden Prairie (1992)

Mrozowski, S.: Electronic properties and band model of carbons. Carbon **9**, 97–109 (1971)

Myglovets, M., Poddubnaya, O., Sevastyanova, O., Lindström, M., Gawdzik, B., Sobiesiak, M., Tsyba, M., Sapsay, V., Klymchuk, D., Puziy, A.: Preparation of carbon adsorbents from lignosulfonate by phosphoric acid activation for the adsorption of metal ions. Carbon **80**, 771–783 (2014)

Neimark, A., Lin, Y., Ravikovitch, P., Thommes, M.: Quenched solid density functional theory and pore size analysis of micro-mesoporous carbons. Carbon. **47**, 1617–1628 (2009)

Ni, D., Shen, H., Li, H., Ma, Y., Zhai, T.: Synthesis of high efficient Cu/TiO_2 photocatalysts by grinding and their size-dependent photocatalytic hydrogen production. Appl. Surf. Sci. **49**, 241–249 (2017)

Oh, Y., Kim, S., Lee, I., Lee, J., Chang, K.: Direct band gap carbon superlattices with efficient optical transition. Phys. Rev. B **93**, 085201-1–085201-8 (2016)

Park, S.-J., Shin, J.-S.: Preparation and characterization of activated carbon/Cu catalyst by electroless copper plating for removal of NO. J. Porous Mater. **11**, 15–19 (2004)

Puziy, A., Poddubnaya, O.: The properties of synthetic carbon derived from nitrogen- and phosphorus-containing polymer. Carbon **36**, 45–50 (1998)

Puziy, A., Poddubnaya, O., Ritter, J., Ebner, A., Holland, C.: Elucidation of the ion binding mechanism in heterogeneous carbon-composite adsorbents. Carbon **39**, 2313–2324 (2001)

Puziy, A., Poddubnaya, O., Ziatdinov, A.: On the chemical structure of phosphorus compounds in phosphoric acid-activated carbon. Appl. Surf. Sci. **252**, 8036–8038 (2006)

Puziy, A., Poddubnaya, O., Socha, R., Gurgul, J., Wisniewski, M.: XPS and NMR studies of phosphoric acid activated carbons. Carbon **46**, 2113–2123 (2008)

Puziy, A., Kochkin, Y., Poddubnaya, O., Tsyba, M.: Ethyl tert-butyl ether synthesis using carbon catalysts from lignocellulose. Adsorpt. Sci. Technol. **35**, 473–481 (2017)

Radovic, L., Moreno-Castilla, C., Rivera-Utrilla, J.: Carbon materials as adsorbents in aqueous solutions. In: Radovic, L.R. (ed.) Chemistry and Physics of Carbon, pp. 227–405. Marcel Dekker, Inc., New York (2000)

Rajagopal, S., Nataraj, D., Khyzhun, O., Djaoued, Y., Robichaud, J., Mangalaraj, D.: Hydrothermal synthesis and electronic properties of $FeWO_4$ and $CoWO_4$ nanostructures. J. Alloys Compd. **493**, 340–345 (2010)

Rauf, M., Ashraf, S.: Fundamental principles and application of heterogeneous photocatalytic degradation of dyes in solution. Chem. Eng. J. **151**, 10–18 (2009)

Rodriguez-Reinoso, F.: The role of carbon materials in heterogeneous catalysis. Carbon **36**, 159–175 (1998)

Rouquerol, J., Llewellyn, P., Rouquerol, F.: Is the BET equation applicable to microporous adsorbents? In: Llewellyn, P.L., Rodriquez-Reinoso, F., Rouqerol, J., Seaton, N. (eds.) COPS-7: Characterization of Porous Solids VII. Studies in Surface Science and Catalysis, vol. 160, pp. 49–56. Elsevier. Amsterdam (2007)

Sangami, G., Dharmaraj, N.: UV–visible spectroscopic estimation of photodegradation of rhodamine-B dye using tin(IV) oxide nanoparticles. Spectrochim. Acta A **97**, 847–852 (2012)

Santos, A., Yustos, P., Cordero, T., Gomis, S., Rodríguez, S., García-Ochoa, F.: Catalytic wet oxidation of phenol on avtive carbon: stability, phenol conversion and mineralization. Catal. Today **102–103**, 213–218 (2005)

Savio, A.K.P.D., Fletcher, J., Smith, K., Iyer, R., Bao, J.M., Robles Hernández, F.C.: Environmentally effective photocatalyst CoO–TiO_2 synthesized by thermal precipitation of Co in amorphous TiO_2. Appl. Catal. B **182**, 449–455 (2016)

Shu, J., Cheng, S., Xia, H., Zhang, L., Peng, J., Li, C., Zhang, S.: Copper loaded on activated carbon as an efficient adsorbent for removal of methylene blue. RSC Adv. **7**, 14395–14405 (2017)

Shukla, P., Wang, S., Sun, H., Ang, M., Tada, H.M.: Activated carbon supported cobalt catalysts for advanced oxidation of organic contaminants in aqueous solution. Appl. Catal. B **100**, 529–534 (2010)

Strelko, V., Kutz, V., Thrower, P.: On the mechanism of possible influence of heteroatoms of nitrogen, boron and phosphorus in a carbon matrix on the catalytic activity of carbons in electron transfer reactions. Carbon **38**, 1499–1524 (2000)

Strelko, V., Kartel, N., Dukhno, I., Kuts, V., Clarkson, R., Odintsov, B.: Mechanism of reductive oxygen adsorption on activated carbons with various surface chemistry. Surf. Sci. **548**, 281–290 (2004)

Sydorchuk, V., Khalameida, S., Zazhigalov, V., Zakutevskii, O.: Some properties of a vanadium molybdenum oxide composite produced by mechanochemical treatment in various media. Russ. J. Inorg. Chem. **58**, 1349–1355 (2013)

Tang, X., Wang, Z., Huang, W., Jing, Q., Liu, N.: Construction of N-doped TiO_2/MoS_2 heterojunction with synergistic effect for enhanced visible photodegradation activity. Mater. Res. Bull. **105**, 126–132 (2018)

Tarkovskaya, I.: Oxidized Carbon. Naukova Dumka, Kyiv (1981) (in Russian)

Thommes, M., Kaneko, K., Neimark, A., Olivier, J., Rodriguez-Reinoso, F., Rouquerol, J., Sing, K.: Physisorption of gases, with special reference to the evaluation of surface area and pore size distribution (IUPAC technical report). Pure Appl. Chem. **87**, 1051–1069 (2015)

Trogadas, P., Fuller, T., Strasser, P.: Carbon as catalyst and support for electrochemical energy conversion. Carbon **75**, 5–42 (2014)

Velasco, L., Fonseca, I., Parra, J., Lima, J., Ania, C.: Photochemical behaviour of activated carbons under UV irradiation. Carbon **50**, 249–258 (2012)

Velasco, L., Maurino, V., Laurenti, E., Fonseca, I., Lima, J., Ania, C.: Photoinduced reactions occurring on activated carbons. A combined photooxidation and ESR study. Appl. Catal. A **452**, 1–8 (2013)

Velasco-Soto, M., Pérez-García, S., Alvarez-Quintana, J., Cao, Y., Nyborg, L., Licea-Jiménez, L.: Selective band gap manipulation of graphene oxide by its reduction with mild reagents. Carbon **93**, 967–973 (2015)

Velo-Gala, I., López-Peñalver, J., Sánchez-Polo, M., Rivera-Utrilla, J.: Activated carbon as photocatalyst of reactions in aqueous phase. Appl. Catal. B **142–143**, 694–704 (2013)

Wang, J., Ng, Y., Lim, Y.-F., Ho, G.W.: Vegetable-extracted carbon dots and their nanocomposites for enhanced photocatalytic H_2 production. RSC Adv. **83**, 44117–44123 (2014)

Wong, S., Ngadi, N., Inuwa, I.M., Hassan, O.: Recent advances in applications of activated carbon from biowaste for wastewater treatment: a short review. J. Clean. Prod. **175**, 361–375 (2018)

Wu, T., Liu, G., Zhao, J., Hidaka, H., Serpone, N.: Photoassisted degradation of dye pollutants. V. Self-photosensitized oxidative transformation of Rhodamine B under visible light irradiation in aqueous TiO_2 dispersions. J. Phys. Chem. B **102**, 5845–5851 (1998)

Xiaoyan, G., Xiaojie, Z., Yincai, T., Yabei, H., Zhang, Y., Yanqin, Z.: Preparation of Cu_2O/AC photocatalysts and their photocatalytic activity in degradation of pyrocatechol. Kinet. Catal. **52**, 672–677 (2011)

Xu, M., Jia, S., Chen, C., Zhang, Z., Yan, J., Guo, Y., Zhang, Y., Zhao, W., Yun, J., Wang, Y.: Microwave-assistant hydrothermal synthesis of SnO_2@ZnO hierarchical nanostructures enhanced photocatalytic performance under visible light irradiation. Mater. Res. Bull. **106**, 74–80 (2018)

Yeh, T.-F., Syu, J.-M., Cheng, C., Chang, T.H., Teng, H.: Graphite oxide as a photocatalyst for hydrogen production from water. Adv. Funct. Mater. **20**, 2255–2262 (2010)

Zabihi, M., Khorasheh, F., Shayegan, J.: Supported copper and cobalt oxides on activated carbon for simultaneous oxidation of toluene and cyclohexane in air. RSC Adv. **5**, 5107–5122 (2015)